Soft Matter

PAPER

View Article Online
View Journal | View Issue

Cite this: *Soft Matter*, 2025, **21**, 3890

Tuning stiffness of mechanical metamaterial unit cells *via* transitions to second-order rigid and pre-stressed states†

Joseph C. Roback,[a] Arya Nagrath,[a] Sameera Kristipati,[a] Christian D. Santangelo*[c] and Ryan C. Hayward *[ab]

Received 7th November 2024,
Accepted 11th April 2025

DOI: 10.1039/d4sm01318b

rsc.li/soft-matter-journal

Mechanical metamaterials have been widely studied for their broad range of exotic mechanical properties, and there is particular interest in imparting these materials with tunability to rationally alter their mechanical response on demand. Here, the concept of second-order rigidity is leveraged to design metamaterials that possess a floppy deformation mode, but that can be rigidified by altering the length of the constituent beams, such that a self-stress emerges and the floppy mode vanishes. This simple change in beam length can also give rise to controllable prestress in the material, allowing for further tuning of the elastic properties. Using a design validated with macroscopic 2D unit cells, a microfabricated 3D lattice material is demonstrated. Due to the generality of the rigidity transition, the design can be expanded to any combination of beam lengths for a given topology. Finally, a temperature-responsive hydrogel is incorporated to access the rigidity transition *in situ*. This design represents a simple and scalable method to assemble mechanical metamaterials with tunable rigidity.

1. Introduction

Mechanical metamaterials derive their unusual mechanical properties from their deliberate structuring as opposed to the bulk properties of the constituent materials.[1] Exotic material properties such as negative effective mass density, negative effective moduli, and negative Poisson's ratio can be enabled by rational design of the periodic unit cells making up metamaterials.[2–5] However, these behaviors have traditionally been static once the metamaterial is fabricated and cannot be tuned or altered on demand. Increasingly, however, the incorporation of responsive or tunable elements has added freedom and functionality, enabling new applications in soft robotics, mechanical computing, and vibration damping.[6–10]

Stiffness modulation in metamaterials is often achieved by manipulation of 'floppy' modes, allowing for deformations that in principle require zero energy. For instance, this can be achieved by taking advantage of jamming transitions in sheets of interlocked octahedral frames,[11] wherein contacts formed between the frame edges as the sheets are placed under confinement results in rigidification, or by making changes in the topological connectivity in networks of beams and hinges,[12,13] whereby creation or destruction of contacts within the network removes or generates a floppy mode. These structures are generally assessed for rigidity by Maxwell constraint counting, which compares the number of degrees of freedom to the number of constraints imposed by contacts;[14] however a theoretical understanding of rigidity through changing self-contact is still under-developed.

Furthermore, many examples of tunable metamaterials rely on tuning mechanisms that are tethered to an external mechanical or pneumatic input,[11,15,16] and can't be triggered remotely. Additional functionality in metamaterial systems can be achieved by implementing tuning mechanisms that are responsive to environmental stimuli such as temperature,[17] light,[18,19] or magnetic field.[20–22] Temperature is a convenient stimulus with a large toolbox of response mechanisms, however, many of the thermally tunable mechanical metamaterials to date rely on shape-memory materials, which require mechanical input for initial high-temperature programming of geometry.[23–25] Alternatively, temperature-induced volume change of hydrogels has been used to trigger inversion of Poisson's ratio *via* a change in unit cell geometry, offering a route to alteration of other mechanical properties as well.[26]

Underconstrained systems that possess one or more degrees of freedom according to Maxwell constraint counting can still be made rigid for certain geometric configurations, a concept

[a] *Department of Chemical and Biological Engineering, University of Colorado Boulder, Boulder, Colorado, 80303, USA. E-mail: ryan.hayward@colorado.edu*
[b] *Materials Science and Engineering Program, University of Colorado Boulder, Boulder, Colorado, 80303, USA. E-mail: ryan.hayward@colorado.edu*
[c] *Department of Physics, Syracuse University, Syracuse, New York, 13244, USA. E-mail: cdsantan@syr.edu*

† Electronic supplementary information (ESI) available. See DOI: https://doi.org/10.1039/d4sm01318b

termed "second-order rigidity."[27] This behavior is observed in disordered spring and fiber networks,[28–32] as well as in more complicated structures such as vertex models.[33,34] The primary phenomenon is a transition from a floppy to a rigid structure upon an apparently subtle change in geometry that requires no change in connectivity or contacts. This broad phenomenon is universal for many systems,[35] and we have used a similar transition to rigidify a chain of interconnected rotors, where changing the lengths of one beam suddenly prevents propagation of motion down the chain.[36] However, to our knowledge, it has not been employed in the design of mechanical metamaterials. One obstacle to achieving such a metamaterial is that second-order rigid systems are currently mainly understood through the length changes of springs, whereas a typical material might have torsional stiffness or the internal buckling of elements.

In this paper, we design a mechanical metamaterial whose shear modulus can be tuned dramatically by changes in the material geometry without a corresponding change in the coordination of the network. Our idea exploits second-order rigidity, where our design is predicted to be floppy according to simple constraint counting but, by changing the length of a subset of the beams such that a prestress is introduced to the network, the metamaterial passes through a critical point where it will suddenly rigidify. We demonstrate that the effect is robust and generic by modeling the response of such networks with and without torsional stiffness at the joints. We fabricate both 2D unit cells and 3D lattice metamaterials to probe their response to shear strain. Finally, a temperature responsive hydrogel is incorporated into the unit cells to drive the transition from floppy-to-rigid *in situ via* a thermal stimulus.

2. Results and discussion

To capitalize on second-order rigidity, we first develop a model of our metamaterial as a system of vertices joined by elastic beams and rotational springs. The floppy modes are the displacements that do not change the length of the beams to first order. However, the floppy modes can be rigidified for certain geometric configurations, such that a small displacement changes the length of the beams to second order, and this occurs even when there is no actual stress on the beams. A more detailed discussion on the conditions for second-order rigidity is given in the ESI† and elsewhere.[27,35] The network's response to deformation is divided into two distinct regimes: when the network lengths are chosen so that the self-stress disappears, the network is floppy. When the network lengths are chosen so that a prestress is realized in the network, the floppy modes disappear, and the system behaves elastically. Precisely between these two regimes is a critical surface indicating the onset of rigidity, which is governed by seemingly subtle changes in the edge lengths rather than a gross change in network connectivity.

Fig. 1(A) shows the design for a simple metamaterial unit cell designed *via* this approach. A square frame of rigid beams contains a network of eight softer beams of the same length. All connections between beams rotate freely. The network is designed so that each unit cell has one degree of freedom (the angle of a specific corner) and shares the symmetry of the square frame to which it is attached, which is symmetric with respect to 90° rotations (when not deformed). When the soft beams are shorter than a critical length l_c the system becomes stressed, and we predict it will behave elastically when the frame is sheared. When the beams are longer than the critical length, however, there is a bifurcation between a clockwise and a counterclockwise rotated configuration and the system becomes floppy, at least up to a critical shear angle. For this specific unit cell geometry, in which all interior beams are of equal length, the critical length is given by $l_c = a/(2+\sqrt{2})$, where a is the side length of the square unit cell. Precisely at the critical length, shear deformations increase the energy quartically (because the strain in the beams is quadratic). Numerical minimization of a spring network with this geometry shows precisely this behavior when the joints are free to rotate (Fig. S3, ESI†).

To accommodate the torsional stiffness of material joints, we add small torsional moduli k_T to all the joints, so that each torsional joint has elastic energy $E_T = k_T(\theta - \theta_0)^2/2$, where θ is the current angle between beams and θ_0 is the angle in equilibrium (Fig. 1(B)). We estimate k_t by 3D printing a single joint that replicates those used in the unit cells below, and placing it under uniaxial tension (see ESI,† Fig. S4 and S5, for details). For small deformations, the restoring force in the floppy state ($l/l_c > 1$) rises more rapidly than in the critical state ($l/l_c = 1$). This can be justified by noting that, in the critical state, the deformation acts to strain the edges whereas, in the floppy state, the joints carry the deformation rather than the edges. However, the restoring force of the floppy geometry rapidly reaches a plateau not observed in the critical state. As the equilibrium length is decreased further ($l/l_c < 1$), the restoring force rises rapidly indicating a substantial stiffening. While prestress is known to induce stiffness in spring networks,[37] here the prestress stiffens without any appreciable geometrical change.

We next experimentally validate the metamaterial design by 3D printing floppy and rigid unit cells using an SLA printer and an elastic resin (Formlabs Elastic 50A). The printed material behaves elastically and has a measured Young's Modulus E = 1.68 MPa (Fig. S6, ESI†). The external frame and interior beams are printed with greater thickness compared to the joints to confine bending to the vertices, and the interior beam lengths for the floppy unit cell are set to be 25% longer than the critical length (l/l_c = 1.25, Fig. 1(C)), while the rigid unit cell's interior beams are set at the critical point geometry (l/l_c = 1, Fig. 1(D)). The printed structures are clamped *via* handles at opposite corners on a force–displacement system, such that uniaxial tension results in shear of the unit cell. Data were recorded with three different test speeds (0.1 cm s^{-1}, 0.25 cm s^{-1}, and 0.5 cm s^{-1}), but we found that the results were nearly

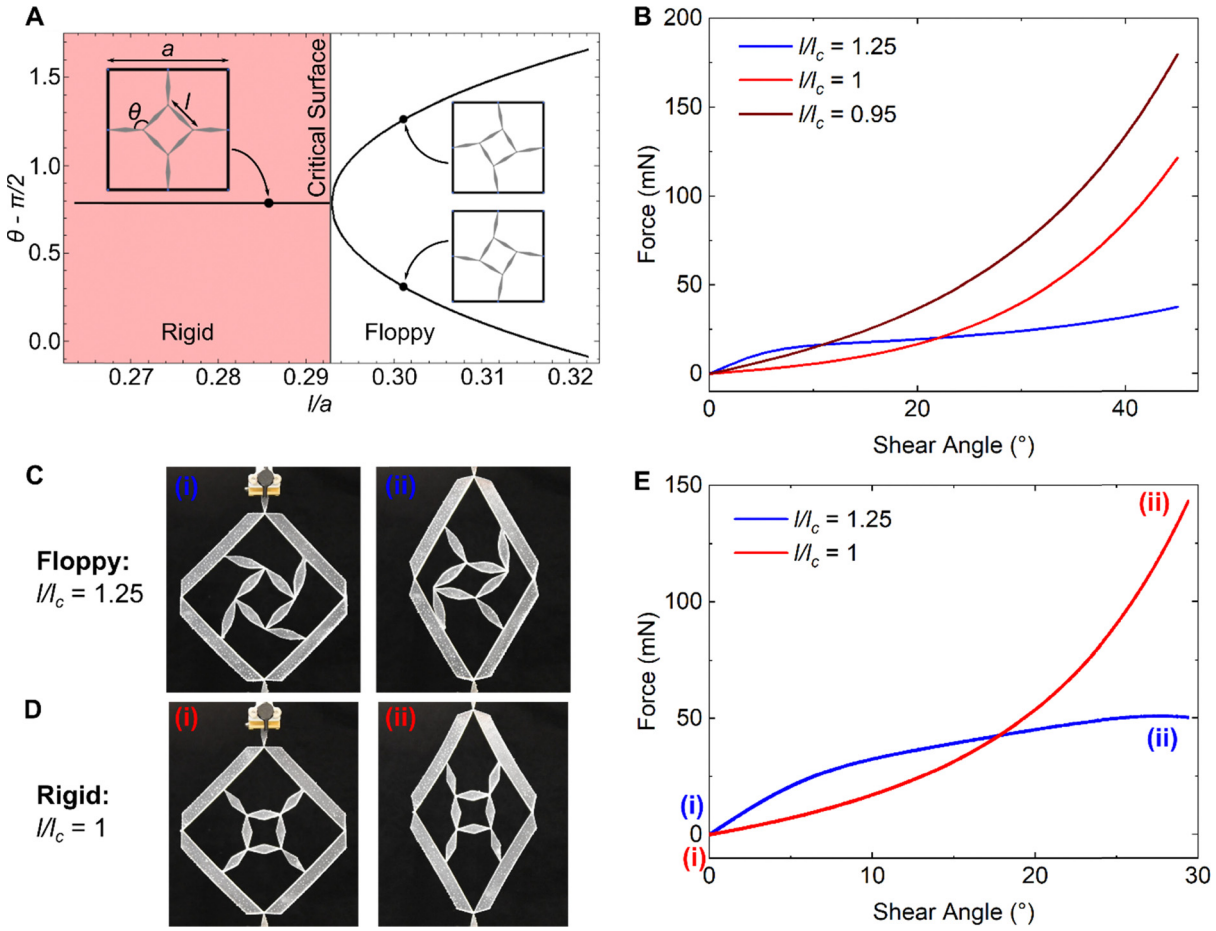

Fig. 1 (A) Phase diagram for the 2nd order rigid unit cell depicted in the insets. (B) Calculated force *vs.* shear response of the unit cell. (C) Photographs of a 3D printed floppy unit cell at (i) zero shear and (ii) 30° shear angle. (D) Photographs of the unit cell with beams shrunk to the critical point at (i) 0° and (ii) 30° shear angle. (E) Force *vs.* shear angle response for rigid and floppy structures.

indistinguishable (Fig. S7, ESI†), indicating that the response was rate independent. Thus, only the slowest speed is plotted for the remainder of this study. The force *vs.* shear angle, where shear angle is defined as the deviation of the frame corner from 90°, is shown in Fig. 1(E). The force response is initially dominated by bending of the joints, and because the floppy unit cell exhibits greater bending at the vertices at small shear strains, it is initially stiffer. However, past ≈10°, the force required to shear the floppy structure increases very weakly compared to the critical geometry, characteristic of the floppy mode predicted by constraint counting, eventually leading to a crossover in the force response. This crossover can be seen as a transition from a bending-dominated to a stretching-dominated deformation mode; however, if one could shrink the joints to zero thickness such that there was no torsional rigidity, the floppy structure would exhibit a true zero-energy mode, and the crossover in force response would vanish (Fig. S8, ESI†). Videos of the mechanical tests are given in supplementary Movie 1 (ESI†).

Building on the results from the single 2D unit cell, we next proceed to fabricate a 3D metamaterial to demonstrate that the concept can be scaled both to smaller spatial dimensions as well as superstructures consisting of multiple unit cells. We employ a cubic unit cell design, where one of the pairs of vertically oriented faces is fabricated with the floppy ($l/l_c = 1.25$) geometry, while the other is at the critical point, thereby creating an anisotropic mechanical metamaterial with a rigid axis and a floppy axis (Fig. 2(A)). We then fabricate the structure in a 3 × 3 × 3 lattice using two-photon lithography (See experimental methods for details), resulting in a structure that is approximately 300 μm on each side. Fig. 2(B) and (C) show scanning electron micrographs of the printed material, where Fig. 2(B) views perpendicular to the floppy axis, and Fig. 2(C) shows the structure rotated 90° to view perpendicular to the rigid axis.

The lattice is mounted on a micromechanical testing system (see methods for experimental details) and sheared by contacting the top of the lattice with a force sensing probe equipped with a flat silicon tip (Fig. 2(D) and supplementary Movie 2, ESI†). The force is recorded as a function of displacement of the stage, which is converted into shear angle using the dimensions of the lattice (Fig. 2(E)). Qualitatively, the same behavior is observed as for the macroscopic, 2D unit cells, where the floppy axis is initially stiffer, but is superseded by the rigid axis at modest shear angles. Due to the limited toughness of the 3D printing resin, which has a manufacturer-reported Young's

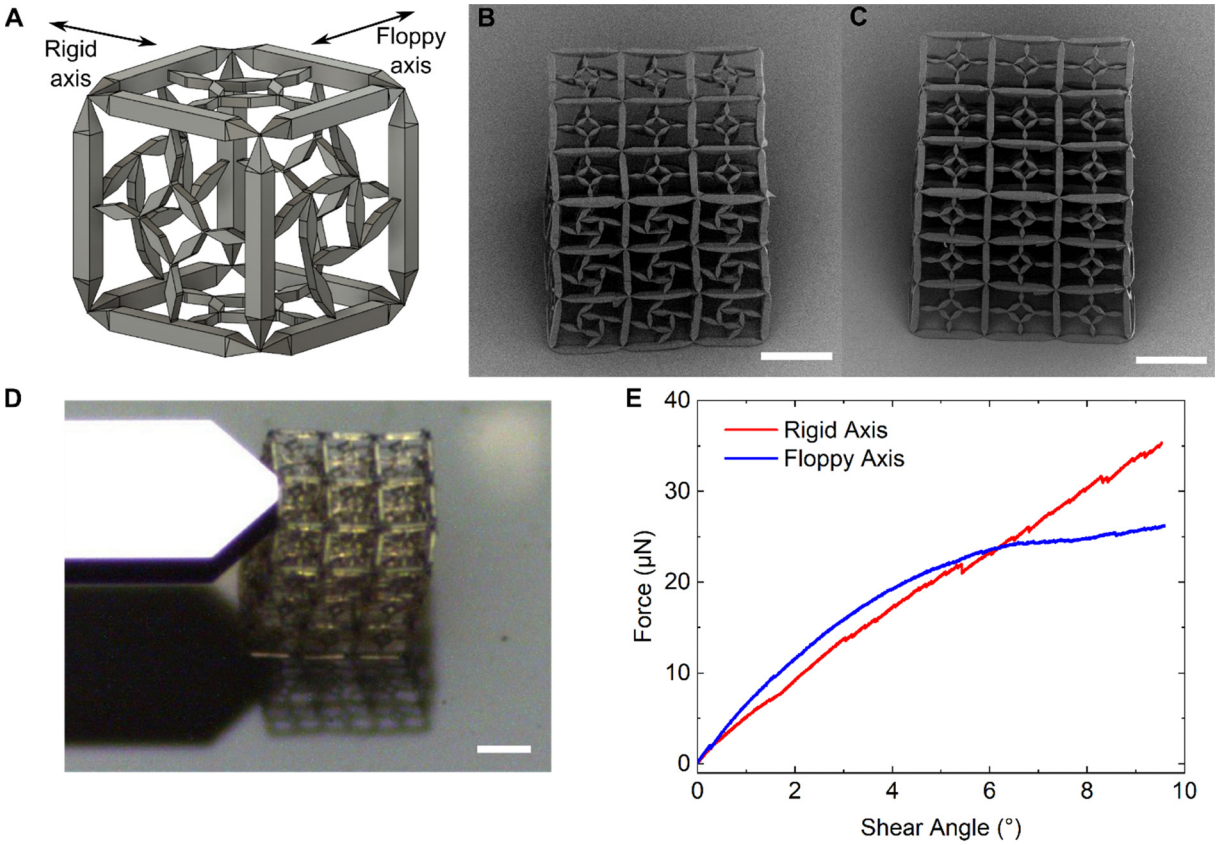

Fig. 2 (A) CAD drawing of single cubic unit cell. (B) Scanning electron micrograph of 3 × 3 × 3 lattice metamaterial viewing the floppy face. (C) Scanning electron micrograph of 3 × 3 × 3 lattice metamaterial that has been rotated 90° to view face designed with the critical point geometry. (D) Optical micrograph of shearing measurement performed by microforce sensing probe. (E) Force *vs.* shear angle shown for measurements along the rigid and floppy axes. Scale bars are 100 μm for all images.

modulus of 1.5 GPa and strain-at-break of 0.7%, the joints tended to fracture at shear angles above ≈10°, restricting the range of accessible shear angles. Also, we observed significant plastic deformation, as evidenced by the large hysteresis in the force response (Fig. S10A, ESI†). Nevertheless, we demonstrate that the second order rigid unit cell design can be assembled into a 3D lattice with the same basic properties, where future work could aim to optimize the structures through material selection, geometry, and printing parameters.

While the approach of 3D printing monolithic, single-component, metamaterials allows for realization of both floppy and rigid responses, as well as structures combining these geometries for anisotropic response, this approach introduces several drawbacks. First, a prestressed configuration cannot be printed monolithically; second, the interior beams cannot be easily made of a different material to introduce tunability; and third, in the floppy case, the interior beams collide with the frame at modest shear values, rigidifying the structure through the formation of additional contacts (Fig. S9, ESI†). We address these shortcomings by instead 3D printing only the interior, and then attaching those beams to a frame made from LEGO Technic pieces (Fig. 3(A) and (B)). This hybrid design enables mechanical testing to higher shear angles (Fig. 3(C) and supplementary Movie 3, ESI†), and critically, displays similar behavior to both the model and the monolithically printed unit cells. In this case, however, the difference in stiffness between the rigid and floppy unit cells is significantly more pronounced, which can be attributed to the use of LEGO pins instead of 3D printed joints, substantially reducing the contribution of bending energy and approaching the limit of a zero-energy mode. Additionally, a set of beams with lengths 5% smaller than the critical value was printed, then stretched to attach to the LEGO frame, leading a built-in prestress within the metamaterial. As seen in Fig. 3(C) (dark red curve), this sample demonstrates an extremely stiff response initially, a feature not present in Fig. 1(B), but then appears to strain soften and displays a response in qualitative agreement with the model predictions. A notable consequence of the use of a LEGO frame is the presences of substantial hysteresis in the force–displacement curves (Fig. S10B, ESI†), which appears to arise from the friction between the LEGO pins and the holes that they rotate in, and is more pronounced under higher tension, since the pins tend to bend and therefore push against the sides of the holes, increasing friction. We speculate that friction is also the cause of the shape of the loading curve in the prestressed sample; however, the exact mechanism is not well understood. Nevertheless, if one compares either the loading or unloading curves across the three samples, it is clear that a dramatic

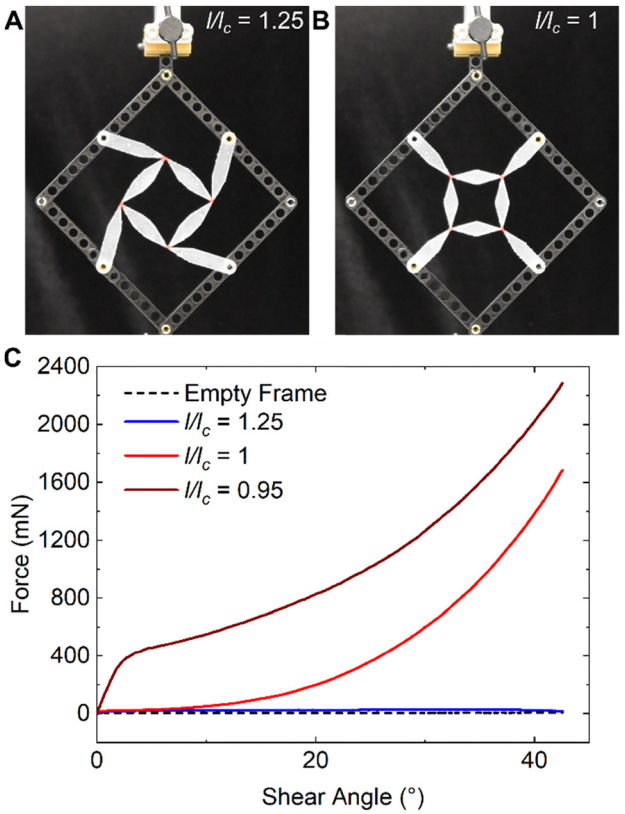

Fig. 3 Photographs of the LEGO/3D printed hybrid unit cell (A) in the floppy geometry and (B) at the critical point. (C) Force *vs.* shear angle for LEGO/3D printed hybrid unit cells.

change in stiffness is achieved simply through variations of beam length by a total of ≈30%.

Next, we highlight the generality of this design approach for networks of a given topology by randomizing the lengths of the beams. A random number generator with a flat distribution between 1.00 and 1.50 is used to select the lengths of the beams in the unit cell interior (Fig. 4(A)); manual shortening of beam 3 was required to maintain sufficiently large joint angles to be 3D printed. Because this structure is beyond the critical point, it again bifurcates into two possible geometries in the same way as the symmetric case. In the case of 8 different beam lengths, this unit cell is now described by an 8-dimensional phase diagram, and the critical manifold is now a 7-dimensional hypersurface.

To find a point on the critical surface, we keep the ratio of lengths for the soft beams but decrease their overall size by a common multiplicative factor while preserving the frame size. If the beam length is decreased enough, the network will clearly carry a self-stress; when the length is sufficiently large, it will be floppy. The critical length occurs precisely at the boundary between these two behaviors. The exact configuration of the network will depend on the ratios between the lengths of the beams but for any choice of ratios, we are guaranteed to reach the critical surface. Consequently, there are many possible options we could have chosen for our design, for which Fig. 4(A) shows precisely one.

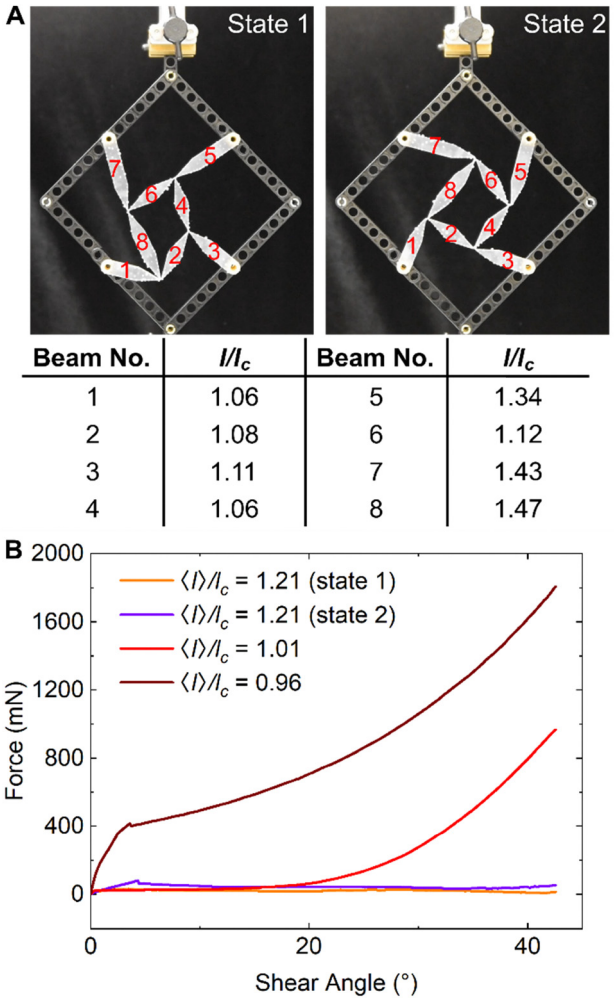

Beam No.	l/l_c	Beam No.	l/l_c
1	1.06	5	1.34
2	1.08	6	1.12
3	1.11	7	1.43
4	1.06	8	1.47

Fig. 4 (A) Photographs of LEGO/3D printed unit cells with randomly generated beams lengths in state 1 (left) and state 2 (right). The beams are numbered on the image and the randomly generated l/l_c values are given in the table below. (B) Force *vs.* shear angle for randomly generated LEGO/3D printed unit cells.

We again print the interior from Formlabs elastic resin, and we describe the beam lengths using the ratio of the average beam length $\langle l \rangle$ to the critical length of the symmetric unit cell l_c. As seen in Fig. 4(B), the unit cell with randomly lengthened beams exhibits floppy behavior in both of its two bifurcated geometries. The state 2 geometry (purple line) exhibits a snap-through on the return curve (Fig. S10C, ESI†), likely arising from the fact the joints are turned opposite from their printed angle. When the beams are shortened to the calculated critical point (corresponding to $\langle l \rangle / l_c = 1.01$), and further shortened to a prestressed state with $\langle l \rangle / l_c = 0.96$, the force responses are again qualitatively similar to the case of equal beam lengths in Fig. 3, showing the generality of the rigidity transition. Videos of the mechanical tests are given in supplementary Movie 4 (ESI†).

Finally, we develop a metamaterial unit cell with an interior made from a responsive material, such that a stimulus can switch the system from floppy to rigid mechanical response on demand. The frame is again assembled from LEGO Technic

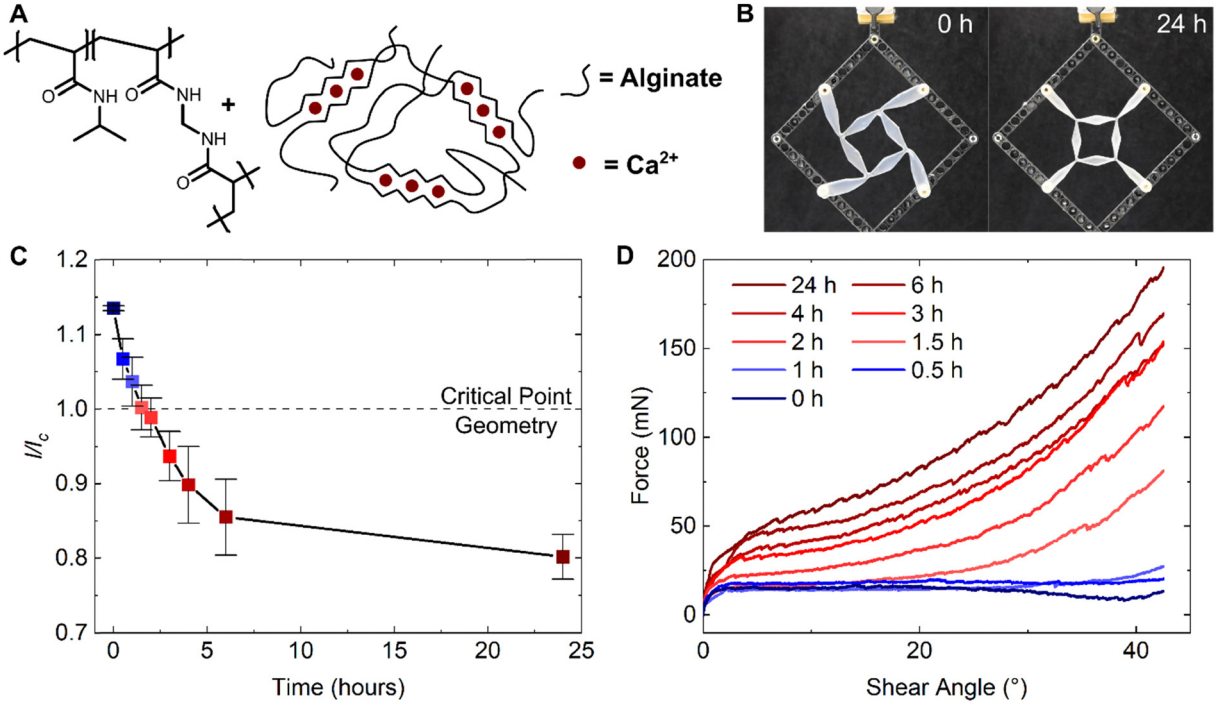

Fig. 5 (A) Chemical structures of NIPAM and calcium crosslinked alginate used to fabricate the hydrogel interior. (B) Photographs of hydrogel/LEGO hybrid unit cell at room temperature swelling equilibrium (left), and after 24 hours of immersion in 34 °C DI water (right). (C) Linear swelling ratio of NIPAM/alginate gels as a function of time immersed in 34 °C DI water. (D) Force *vs.* shear angle for hydrogel/LEGO hybrid unit cells taken at several different times of immersion in 34 °C DI water.

beams; however, the interior is now made from a poly (*N*-isopropylacrylamide)/alginate double network hydrogel (Fig. 5(A), see Experimental section for a detailed procedure). In brief, a mold is 3D printed to match the critical point geometry (l/l_c = 1), and the pre-gel solution consisting of *N*-isopropylacrylamide (NIPAM), *N*,*N*′-methylenebisacrylamide, sodium alginate, and lithium phenyl-2,4,6-trimethylbenzoyl phosphinate in water is added to the mold and cured under UV illumination. The mold is then immersed in $CamathCl_2$ solution to ionically crosslink the alginate, then the hydrogel interior was removed from the mold and swollen to equilibrium in DI water before being attached to the frame *via* LEGO pins. We note that a similar strategy was employed to fabricate hydrogel metamaterials with tunable Poisson's ratio.[26] The monomer and crosslinker concentrations are chosen such that the structure is stiff enough to display minimal deformation under gravity, yet still swells enough at room temperature to pass beyond the critical point. Additionally, the use of an interpenetrating alginate network was necessary to render the material sufficiently tough to endure removal from the mold and subsequent mechanical testing without breaking the thin joints.

The unit cell is sheared at room temperature, after reaching swelling equilibrium, where the linear swelling ratio corresponds to $l/l_c \approx 1.14$. The structure displayed the floppy response indicative of being above the critical point (Fig. 5(C) and (D), dark blue). The unit cell is then immersed in 34 °C DI water and removed periodically to measure the swelling ratio and the force response to shear. The time-dependent linear swelling ratio is shown in Fig. 5(C), where the dashed line at l/l_c = 1 represents the "as-prepared" critical point geometry. The hydrogel interior beams cross this line after approximately 90 min, and a corresponding change in the force response from floppy to rigid is observed (Fig. 5(D)). As the unit cell is left longer in the warm water, the interior continues to shrink into a prestressed state, and the stiffness increases further, qualitatively consistent with the 3D-printed prestressed samples. These results indicate that controlling the prestress is another powerful tool for altering the elastic properties of the unit cell. For example, taking one measure of the modulus to be the slope of the loading curve around a shear angle of 20 degrees, we find that this "incremental modulus" increases by approximately a factor of 4 between the critical point (1.5 h) and the fully deswollen state (24 h) (Fig. S12, ESI†). Force displacement curves with unloading data are shown in Fig. S10D (ESI†), additional images are shown in Fig. S11 (ESI†), and videos of the mechanical tests are given in supplementary Movie 5 (ESI†). This responsive hydrogel design exemplifies the *in situ* tunability of this metamaterial design *via* temperature-induced rigidification, without the need for external mechanical input. An alternative design for tuning stiffness in hydrogels involves the use of stored length arising from buckling of swollen elements, where the onset of strain-stiffening occurs when the buckled beams are pulled straight into the plane of the frame.[38] The strategy introduced in this work allows for modulating the onset of shear stiffening by many tens of degrees

from changes in beam length of only a few percent (Fig. 5(D) and Fig. S3, ESI†), and has the additional advantage of exhibiting a near-zero-stiffness mode beyond the critical point.

3. Conclusion

In this work, we introduce a concept for a mechanical metamaterial with a tunable shear modulus, which can be realized by altering the length of the constituent beams in such way that the structure possesses a self-stress. The developed unit cells possess a floppy deformation mode until the interior beams are shrunk to a critical length, at which point the material is second-order rigid. The behavior is well-described by a model system of linear and torsional springs, which must be added to simulate the effects of non-zero joint stiffness. We further demonstrate that the single 2D unit cells can be assembled into 3D lattices that can be fabricated on the micron scale and maintain the same qualitative behavior; however, due to material limitations, were prone to plasticity and fracture. Further work could aim to optimize printing parameters for an elastomeric two-photon resin, or to incorporate responsive hydrogel elements using a mulitmaterial two-photon lithographic approach Such designs would allow for micron-scale superstructures with drastically tunable stiffness in multiple directions with potential applications in soft robotics or acoustic manipulation.

The effect of prestress, as well as generalization of the concept to randomly generated beam lengths were shown by combining 3D printed interior beams with a LEGO frame. In this work, we outlined a single simple network topology; however, this concept can be expanded for spring networks of any topology possessing an analagous floppy mode. Future work could aim to explore more complicated network architectures, further explore the effects of prestress on modulus, and optimize for metamaterial properties such as stiffness of the rigid phase and onset of strain stiffening. Finally, we leverage the temperature responsiveness of NIPAM hydrogels to alter the rigidity of the unit cell *in situ via* a change in temperature. Overall, we anticipate that this work serves as a demonstration for a simple, and generalizable platform for the design of functional mechanical metamaterials.

4. Experimental section/methods

Materials

N-Isopropylacrylamide (NIPAM) was purchased from TCI and was recrystallized from hexanes prior to use. All other materials were purchased from commercial sources and used as received.

Numerical simulations of metamaterial structures

The structures were represented as graphs of vertices joined by edges and simulated using a custom-built Mathematica (v13.3) package (**https://github.com/cdsantan/mechanisms**). Elements were modeled as springs with stretching energy $E_{\text{spring}} = k_{\text{spring}}(l - l_0)^2/2$ where l is the spring length, l_0 the equilibrium length, and k_{spring} the spring constant. Joints were modeled with torsional energy $E_{\text{torsional}} = k_{\text{torsional}}(\theta - \theta_0)^2/2$ where θ is the joint angle, θ_0 its corresponding equilibrium angle, and $k_{\text{torsional}}$ is the torsional modulus of the joint. For each shear angle of the frame, the vertex positions of the frame are fixed and the elastic energy is minimized with respect to the position of the vertices. Values of the spring and torsional constants were estimated by comparing to force–displacement measurements of individual bars and torsional springs (ESI†). Additional Mathematica code can be found in the ESI.†

3D printing of 2D unit cells

CAD files were generated using Fusion 360 (Autodesk), and designs were printed on either a Form 2 or Form 3+ 3D printer using elastic 50A resin (Formlabs). Printed designs were washed in fresh isopropanol twice for 20 min each, and thermally post-cured in an 80 °C oven overnight.

Force–displacement testing of 2D unit cells

Unit cells were clamped at opposite corners on a TA.XTplus Texture Analyzer (Stable Micro Systems) equipped with a 500 g load cell. Unit cells were clamped such that the initial angle of the joints was 90°. Samples were deformed in tension at 0.1 cm s^{-1}, 0.25 cm s^{-1}, and 0.5 cm s^{-1} to a maximum of 4 cm, then returned to their starting position. Linear displacements were converted to shear angles using the geometry of the unit cell.

3D printing of microscale 3D lattices

Fused silica substrates (Nanoscribe GbmH) were first cleaned by ultrasonication in DI water, acetone, and isopropanol for 10 min each, then by treating with UV-ozone cleaning for 10 min per side. A solution of 1 mL of the adhesion promoter 3-(trimethoxysilyl)propyl methacrylate in 200 mL of ethanol was prepared, then 6 mL of 1 : 10 glacial acetic acid : water was added. The clean substrates were immersed in this solution for 15 min, then rinsed with isopropanol to functionalize the surface with methacrylate units and improve adhesion of the printed structures. CAD files were generated using Fusion 360 (Autodesk). Structures were fabricated on a Nanoscribe Photonic Professional GT2 (Nanoscribe GbmH) using a 63× NA1.4 objective and IP-Dip2 resin in dip-in mode. The laser power was set to 50% and the scan speed was set to 15 000 μm s^{-1}. Fabricated structures were developed in SU-8 developer, then transferred to isopropanol. Without allowing them to dry, the structures were then placed in an EM CPD300 critical point dryer (Leica Microsystems) to remove the solvent using supercritical CO_2 and avoid structural collapse due to surface tension.

Imaging of microscale 3D lattices

The metamaterial lattice structures were sputtered with 4 nm of platinum using a 108 Auto/SE sputter coater (Cressington), then imaged using a TM-4000PlusE-2 scanning electron microscope (Hitachi) using secondary electrons and an accelerating voltage of 10 kV.

Force–displacement testing of microscale 3D lattices

The fused silica substrate was scribed and broken such that the lattice was positioned approximately 1–2 mm from the edge of the substrate on 2 perpendicular faces. The sample was mounted on a FT-MTA03 micromechanical testing system (FemtoTools AG) by supergluing the substrate to a custom 3D-printed post, which was in turn superglued to the instrument's sample mount. A microforce sensing probe with a flat silicon tip and a max force capacity of 20 mN was aligned with the top center of the lattice using the onboard camera. Compression tests were then carried out on the lattice with a test speed of 0.25 μm s^{-1} and the force response was measured. Since the probe was aligned with the top of the lattice with the bottom fixed to the substrate compression resulted in shear of the lattice. The displacement was converted to shear angle using the sample height.

Fabrication of NIPAM/LEGO hybrid unit cell

A modified procedure from ref. 26 was used. First, a mold matching the critical point geometry was 3D printed using flexible 80A resin (Formlabs). Then, 2.263 g (20 mmol) of *N*-isopropylacrylamide, 62 mg (0.4 mmol) of *N*,*N*-methylenebisacrylamide, and 22.5 mg (0.08 mmol) of lithium phenyl-2,4,6-trimethylbenzoylphosphinate were dissolved in 20 mL of DI water, sparged with nitrogen gas for 30 min, and cooled to 0 °C in an ice bath. The solution was then poured into the mold, LEGO pins were placed in the vertices, and the solution was cured under a 365 nm lamp (Melodie Suzie 36 W) for 3 min. The entire mold was immersed in 0.2 M $CaCl_2$ for 24 h, then the gel was carefully removed from the mold, and immersed again in 0.2 M $CaCl_2$ for an additional 48 h to ensure full ionic crosslinking. Finally, the gel was attached to the LEGO frame, and immersed in DI water for 3 d to reach swelling equilibrium. Force displacement testing was conducted in the same way as the 3D printed samples above.

Author contributions

J. C. R., C. D. S., and R. C. H. conceived and/or designed the research. J. C. R., A. N., and S. K. conducted the experiments. C. D. S. conducted theory, computation, and modelling. J. C. R., C. D. S., and R. C. H. wrote and revised the manuscript. C. D. S. and R. C. H. supervised the work. All authors have given approval to the final version of the manuscript.

Data availability

The data that support the findings of this work are available in the manuscript or the ESI.† Raw research data is available on reasonable request for the corresponding author.

Conflicts of interest

The authors declare no conflicts of interest.

Acknowledgements

This work was supported by the National Science Foundation through grant CMMI 2247094 and made use of equipment acquired *via* grant N00014-21-1-2836 from the Office of Naval Research. We also acknowledge the Colorado Shared Instrumentation in Nanofabrication and Characterization (COSINC) for providing cleanroom and SEM facilities.

References

1 J.-H. Lee, J. P. Singer and E. L. Thomas, Micro-/Nanostructured Mechanical Metamaterials, *Adv. Mater.*, 2012, **24**, 4782–4810.
2 M. Kadic, T. Bückmann, N. Stenger, M. Thiel and M. Wegener, On the practicability of pentamode mechanical metamaterials, *Appl. Phys. Lett.*, 2012, **100**, 191901.
3 Z. Liu, X. Zhang, Y. Mao, Y. Y. Zhu, Z. Yang, C. T. Chan and P. Sheng, Locally Resonant Sonic Materials, *Science*, 2000, **289**, 1734–1736.
4 T. Bückmann, N. Stenger, M. Kadic, J. Kaschke, A. Frölich, T. Kennerknecht, C. Eberl, M. Thiel and M. Wegener, Tailored 3D Mechanical Metamaterials Made by Dip-in Direct-Laser-Writing Optical Lithography, *Adv. Mater.*, 2012, **24**, 2710–2714.
5 R. Schittny, T. Bückmann, M. Kadic and M. Wegener, Elastic measurements on macroscopic three-dimensional pentamode metamaterials, *Appl. Phys. Lett.*, 2013, **103**, 231905.
6 K. Bertoldi, V. Vitelli, J. Christensen and M. van Hecke, Flexible mechanical metamaterials, *Nat. Rev. Mater.*, 2017, **2**, 1–11.
7 J. Shintake, V. Cacucciolo, D. Floreano and H. Shea, Soft Robotic Grippers, *Adv. Mater.*, 2018, **30**, 1707035.
8 J. A. Faber, A. F. Arrieta and A. R. Studart, Bioinspired spring origami, *Science*, 2018, **359**, 1386–1391.
9 A. Rafsanjani, K. Bertoldi and A. R. Studart, Programming soft robots with flexible mechanical metamaterials, *Sci. Robot.*, 2019, **4**, eaav7874.
10 M. Kheybari, C. Daraio and O. R. Bilal, Tunable auxetic metamaterials for simultaneous attenuation of airborne sound and elastic vibrations in all directions, *Appl. Phys. Lett.*, 2022, **121**, 081702.
11 Y. Wang, L. Li, D. Hofmann, J. E. Andrade and C. Daraio, Structured fabrics with tunable mechanical properties, *Nature*, 2021, **596**, 238–243.
12 M. A. Wagner, F. Schwarz, N. Huber, L. Geistlich, H. Galinski and R. Spolenak, Deformation-induced topological transitions in mechanical metamaterials and their application to tunable non-linear stiffening, *Mater. Des.*, 2022, **221**, 110918.
13 L. Wu and D. Pasini, Zero modes activation to reconcile floppiness, rigidity, and multistability into an all-in-one class of reprogrammable metamaterials, *Nat. Commun.*, 2024, **15**, 3087.
14 C. L. Kane and T. C. Lubensky, Topological boundary modes in isostatic lattices, *Nat. Phys.*, 2014, **10**, 39–45.

15 X. Fang, J. Wen, L. Cheng, D. Yu, H. Zhang and P. Gumbsch, Programmable gear-based mechanical metamaterials, *Nat. Mater.*, 2022, **21**, 869–876.
16 X. Tan, S. Chen, B. Wang, J. Tang, L. Wang, S. Zhu, K. Yao and P. Xu, Real-time tunable negative stiffness mechanical metamaterial, *Extreme Mech. Lett.*, 2020, **41**, 100990.
17 M. Zhang, A. Pal, Z. Zheng, G. Gardi, E. Yildiz and M. Sitti, Hydrogel muscles powering reconfigurable micro-metastructures with wide-spectrum programmability, *Nat. Mater.*, 2023, 1–10.
18 A. S. Gliozzi, M. Miniaci, A. Chiappone, A. Bergamini, B. Morin and E. Descrovi, Tunable photo-responsive elastic metamaterials, *Nat. Commun.*, 2020, **11**, 2576.
19 H. Patel, J. Chen, Y. Hu and A. Erturk, Photo-responsive hydrogel-based re-programmable metamaterials, *Sci. Rep.*, 2022, **12**, 13033.
20 S. Roh, L. B. Okello, N. Golbasi, J. P. Hankwitz, J. A.-C. Liu, J. B. Tracy and O. D. Velev, 3D-Printed Silicone Soft Architectures with Programmed Magneto-Capillary Reconfiguration, *Adv. Mater. Technol.*, 2019, **4**, 1800528.
21 C. Ma, S. Wu, Q. Ze, X. Kuang, R. Zhang, H. J. Qi and R. Zhao, Magnetic Multimaterial Printing for Multimodal Shape Transformation with Tunable Properties and Shiftable Mechanical Behaviors, *ACS Appl. Mater. Interfaces*, 2021, **13**, 12639–12648.
22 S. M. Montgomery, S. Wu, X. Kuang, C. D. Armstrong, C. Zemelka, Q. Ze, R. Zhang, R. Zhao and H. J. Qi, Magneto-Mechanical Metamaterials with Widely Tunable Mechanical Properties and Acoustic Bandgaps, *Adv. Funct. Mater.*, 2021, **31**, 2005319.
23 C. Yang, M. Boorugu, A. Dopp, J. Ren, R. Martin, D. Han, W. Choi and H. Lee, 4D printing reconfigurable, deployable and mechanically tunable metamaterials, *Mater. Horiz.*, 2019, **6**, 1244–1250.
24 R. Tao, L. Xi, W. Wu, Y. Li, B. Liao, L. Liu, J. Leng and D. Fang, 4D printed multi-stable metamaterials with mechanically tunable performance, *Compos. Struct.*, 2020, **252**, 112663.
25 L. Ren, W. Wu, L. Ren, Z. Song, Q. Liu, B. Li, Q. Wu and X. Zhou, 3D Printing of Auxetic Metamaterials with High-Temperature and Programmable Mechanical Properties, *Adv. Mater. Technol.*, 2022, **7**, 2101546.
26 O. Skarsetz, V. Slesarenko and A. Walther, Programmable Auxeticity in Hydrogel Metamaterials via Shape-Morphing Unit Cells, *Adv. Sci.*, 2022, **9**, 2201867.
27 R. Connelly and W. Whiteley, Second-Order Rigidity and Prestress Stability for Tensegrity Frameworks, *SIAM J. Discrete Math.*, 1996, **9**, 453–491.
28 M. Wyart, H. Liang, A. Kabla and L. Mahadevan, Elasticity of Floppy and Stiff Random Networks, *Phys. Rev. Lett.*, 2008, **101**, 215501.
29 J. Feng, H. Levine, X. Mao and L. M. Sander, Nonlinear elasticity of disordered fiber networks, *Soft Matter*, 2016, **12**, 1419–1424.
30 A. Sharma, A. J. Licup, K. A. Jansen, R. Rens, M. Sheinman, G. H. Koenderink and F. C. MacKintosh, Strain-controlled criticality governs the nonlinear mechanics of fibre networks, *Nat. Phys.*, 2016, **12**, 584–587.
31 F. Burla, J. Tauber, S. Dussi, J. van der Gucht and G. H. Koenderink, Stress management in composite biopolymer networks, *Nat. Phys.*, 2019, **15**, 549–553.
32 M. Merkel, K. Baumgarten, B. P. Tighe and M. L. Manning, A minimal-length approach unifies rigidity in underconstrained materials, *Proc. Natl. Acad. Sci. U. S. A.*, 2019, **116**, 6560–6568.
33 J.-A. Park, L. Atia, J. A. Mitchel, J. J. Fredberg and J. P. Butler, Collective migration and cell jamming in asthma, cancer and development, *J. Cell Sci.*, 2016, **129**, 3375–3383.
34 M. Merkel and M. L. Manning, A geometrically controlled rigidity transition in a model for confluent 3D tissues, *New J. Phys.*, 2018, **20**, 022002.
35 O. K. Damavandi, V. F. Hagh, C. D. Santangelo and M. L. Manning, Energetic rigidity. I. A unifying theory of mechanical stability, *Phys. Rev. E*, 2022, **105**, 025003.
36 M. Berry, D. Limberg, M. E. Lee-Trimble, R. Hayward and C. D. Santangelo, Controlling the configuration space topology of mechanical structures, *Phys. Rev. E*, 2022, **106**, 055002.
37 S. Guest, The stiffness of prestressed frameworks: A unifying approach, *Int. J. Solids Struct.*, 2006, **43**, 842–854.
38 O. Skarsetz, R. Mathes, R. S. Schmidt, M. Simon, V. Slesarenko and A. Walther, Hard- and Soft-Coded Strain Stiffening in Metamaterials *via* Out-of-Plane Buckling Using Highly Entangled Active Hydrogel Elements, *ACS Appl. Mater. Interfaces*, 2024, **16**, 38511–38519.

